Paper:

Surface Formation Behaviors in Wavy Microgroove Cutting on Various Workpiece Materials

Toshitaka Terabayashi and Jiwang Yan[†]

Department of Mechanical Engineering, Faculty of Science and Technology, Keio University
3-14-1 Hiyoshi, Kohoku-ku, Yokohama, Kanagawa 223-8522, Japan
[†]Corresponding author, E-mail: yan@mech.keio.ac.jp
[Received September 11, 2019; accepted October 9, 2019]

Functional films with multi-directional wavy microgrooves can be applied to reduce fluid drag in turbulent flow applications. For high-efficiency mass production of functional films through polymer imprinting, it is necessary to machine wavy microgrooves on the surfaces of metal roll molds. When wavy grooves are cut, to reduce the follow-up errors of machine tools, a very low cutting speed is normally used, but the mechanism of this cutting is still unclear. In this study, microgrooving experiments were conducted on three different workpiece materials: brass, oxygen free copper, and aluminum alloy, and their cutting mechanisms were investigated. Distinct differences in chip formation behavior and machined surface integrity were identified among these materials. Aluminum alloy was chosen as the most suitable material for roll mold fabrication. Two-directional wavy microgrooves with form accuracy on 1 μm level and surface roughness of less than 10 nm *Ra* were obtained.

Keywords: wavy groove, micro cutting, roll mold, workpiece material, functional surface

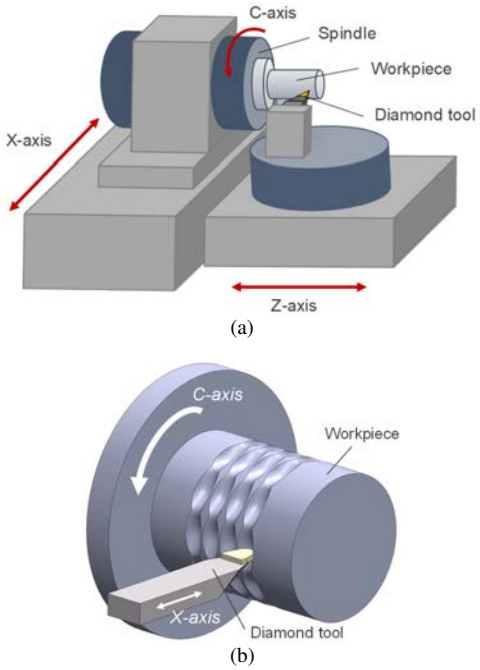

Fig. 1. Schematics of (a) diamond turning machine equipped with slow tool servo; (b) wavy groove cutting on a roll mold by means of *X*-axis tool oscillation.

1. Introduction

Polymer films that have microstructures on their surfaces are being increasingly sought after in industry. Functional films with wavy microstructures and riblets are useful on hydrodynamic parts, as they significantly reduce fluid resistance [1–5]. In order to use polymer imprinting mass produce functional films highly efficiently, wavy microgrooves must be machined on the surfaces of metal roll molds [6, 7]. Using diamond turning with a slow tool servo (STS) is an effective way to obtain these wavy microstructures with high form accuracy and surface quality [8–10]. However, it is not yet clear what material is suitable for fabricating the roll molds. There have been no comparative studies done on the machinability of various workpiece materials for wavy groove cutting, although many studies have been done on diamond turning other kinds of microstructures, including micro prisms, micro lenses, and micro pyramid arrays [11–15].

In wavy groove cutting using an STS, the cutting speed is very low in order to avoid machine tool follow-up errors. Also, the changes in tool position cause changes in tool rake angles and relief angles along with the movement of the STS system, making the cutting mechanism more complicated. Furthermore, in groove cutting, there is no "burnishing effect" induced by multiple traverse tool feeds, so surface defects are difficult to eliminate.

In this study, an ultraprecision machine tool with an STS system was used to machine wavy microgrooves on three different metal materials, namely, brass, oxygen-free copper, and aluminum alloy. The machinability of each metal material was investigated by characterizing the machined surface topography and chip formation behavior under dry and wet conditions.

1.1. Machining Method and Setup

Figure 1(a) is a schematic diagram of a diamond turn-

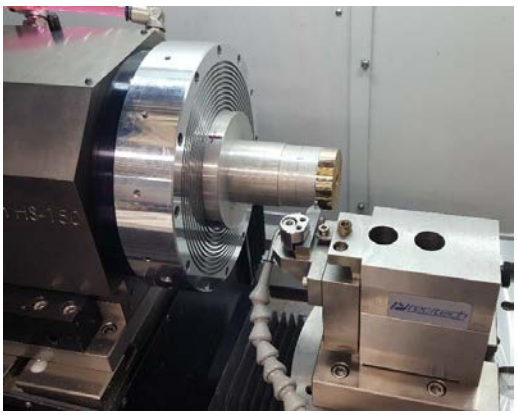

Fig. 2. Photograph of the main section of experimental setup.

Table 1. Cutting conditions.

Spindle rotation rate [rpm]	5
Depth of cut per pass [μm]	1
Cutting speed [m/min]	0.39, 0.78
Workpiece diameter [mm]	25, 50
Coolant	Oil mist
Cutting tool	
Material	Single-crystal diamond
Nose radius [mm]	0.1
Rake angle [deg]	0
Relief angle [deg]	6

ing machine with an STS system, and **Fig. 1(b)** is a schematic of wavy groove cutting on a roll mold performed by oscillating the diamond tool along the X-axis. In STS turning, X- and Z-axes positions of the tool are synchronized with C-axis rotation of the workpiece. To generate wavy microgrooves, the tool is driven along the X- and Z-axes simultaneously to follow dual sinusoidal tool paths.

An ultraprecision diamond turning lathe, Precitech Nanoform X (AMETEK Precitech Inc., USA), having an STS system, was used in the cutting experiments. **Fig. 2** is a photograph of the main section of the machine. A single-crystal diamond tool with a nose radius of 0.1 mm, a rake angle of 0°, and a relief angle of 6° was used. Metal cylinders measuring 25 mm and 50 mm in diameter and 40 mm in length were used as workpieces. Wet cutting was done with an oil mist used for lubrication and cooling; dry cutting was also being done for comparison. The cutting conditions are summarized in **Table 1**. Before the grooving tests, the roll surfaces were diamond-turned to obtain a mirror finish.

As shown in **Fig. 3**, the cross section of a groove is defined by the tool contour. In this study, the depth of cut per tool pass was set to 1 μm. Thus, 20 tool passes (20 spindle revolutions) were needed to obtain a 20 μm-deep microgroove.

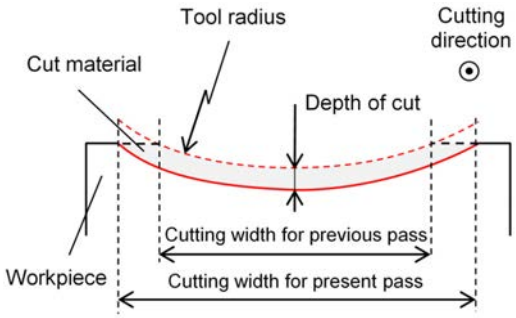

Fig. 3. Cross-sectional view of tool-workpiece contact.

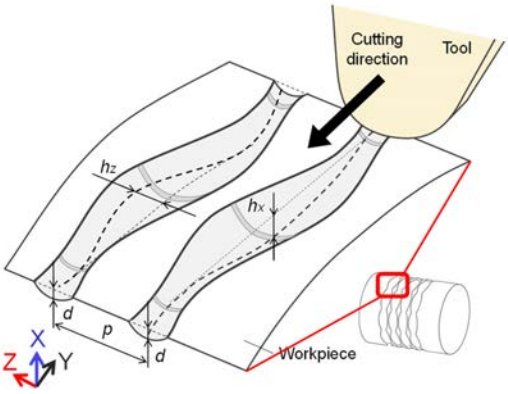

Fig. 4. Schematic of design parameters for compound (C) wavy groove cutting.

Table 2. Wavy groove design.

Wavy shape	A	R	C
Groove depth d [μm]	20	5–25	5–25
X-axis amplitude h_x [μm]	0	20	20
Z-axis amplitude h_z [μm]	20	0	20
Wavelength l [mm]	1.57	1.57	1.57
Groove pitch p [mm]	0.22	0.22	0.22
Number of waves	100	100	100

In this paper, the wavy groove generated by means of X-axis tool oscillation is defined as a radial (R) wave, and one generated by means of Z-axis tool oscillation is defined as an axial (A) groove. The hybrid wavy groove generated through simultaneous X- and Z-axes motions is defined as a compound (C) groove. **Fig. 4** shows design parameters for the type C wavy grooves, and **Table 2** lists the parameter values for the three types of grooves used in this study. The parameter values were selected to be useable for surface riblets that can reduce fluid resistance [1–5].

1.2. Workpiece Materials

The workpieces for roll mold fabrication were made from three metal materials: brass, oxygen-free copper (OFC), and aluminum alloy (AA). The mechanical

Table 3. Material properties.

Materials	Brass	OFC	AA
Chemical composition	Cu-Zn-Pb-Fe-Sn (Cu 61%)	Pure Cu (Cu 99.6%)	Al-Mg (Al 95%)
Hardness [HV]	130	60	60
Young's modulus [kN/mm^2]	96	118	68
Tensile strength [N/mm^2]	420	250	230
Shear strength [N/mm^2]	295	160	221
Extension coefficient [%]	25	20	12

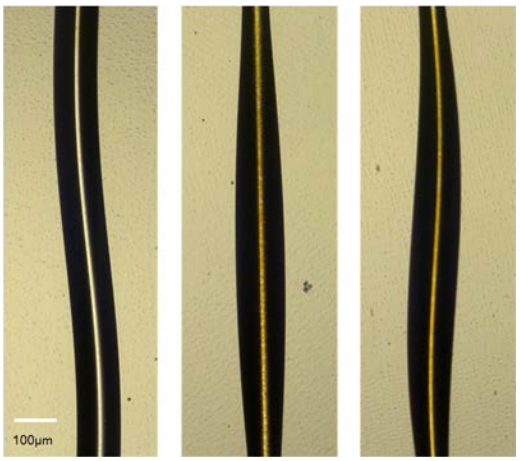

Fig. 5. Micrograph of three kinds of wavy grooves dry machined on brass.

properties of these materials are listed in **Table 3**. Although these materials have been popularly used in diamond turning for optical components, there have been no direct comparisons of the machinability of these materials in micro grooving, especially for the micro cutting of wavy grooves at a low cutting speed.

2. Results and Discussion

2.1. Machining Characteristics of Brass

Figure 5 is a micrograph of three kinds of grooves machined on brass in dry cutting. The groove edges are sharply generated without burr formation, even under dry conditions. However, in the SEM photograph of the groove bottom in **Fig. 6(a)**, grain boundaries and defects are visible on the groove surface. **Fig. 6(b)** is a magnified view of the surface defects. There are deep pits in the surface. These kinds of grain boundaries and pit defects were not observed in diamond turning of a brass cylindrical surface at a higher cutting speed (236 m/s) with a traverse tool feed.

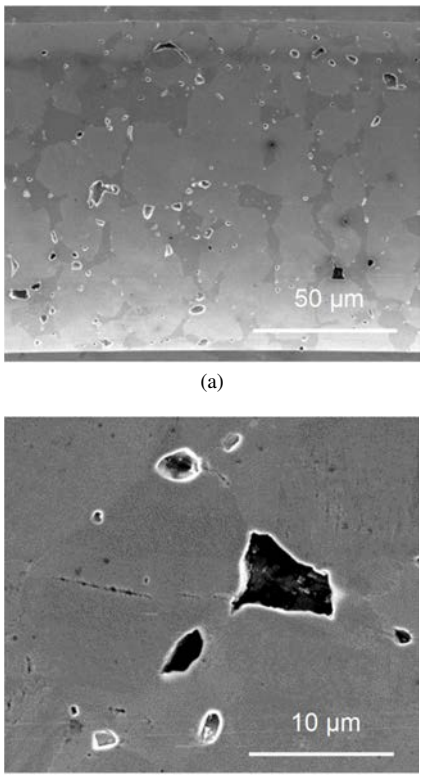

Fig. 6. SEM micrographs of a dry-cut groove: (a) general view and (b) close-up view.

Figure 7(a) is an SEM micrograph of type A grooves wet machined on brass, and **Fig. 7(b)** is a close-up view of the groove bottom. Similar to **Fig. 6**, grain boundaries and pit defects are seen on the groove surface, but grain boundary steps are more clearly seen than in **Fig. 6**. **Fig. 7(c)** is a cross-sectional profile of a groove measured with a white-light interferometer. The grain boundary steps and pits have caused significant surface profile deviations. The surface roughness is about 50 nm *Ra* (300 nm *Rz*).

These results show that the surface topography of brass is less dependent on the presence of a lubricant and much more dependent on the cutting speed. As the cutting speed in wavy groove machining is very slow (< 1 m/min), the deformation behavior of each crystal grain is different, causing clear boundary step formation. Some of the crystal grains or material phases are pulled out from the surface of the workpiece, forming deep pits. Unlike in face turning, in groove cutting there are no "burnishing effects" induced by multiple traverse tool feeds, so the boundary steps and pit defects are not flattened by subsequent tool passes.

Figure 8 is an SEM photograph of cutting chips generated during the cutting of type R grooves. The length of each chip unit is about 500 μm, $1/3$ of a groove period (1.57 mm), and their thickness is generally uniform. These chips indicate that the chip flow is fluent, without severe friction or chip stagnation on the tool rake face, as

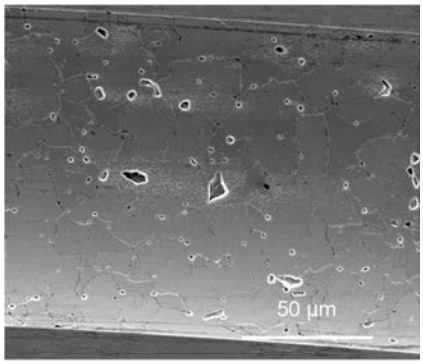

(a)

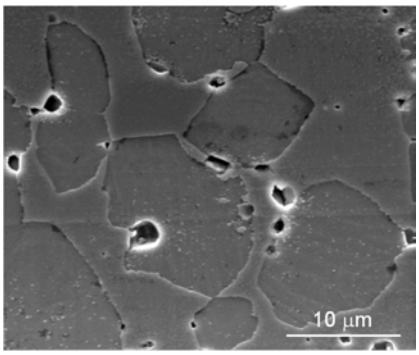

(b)

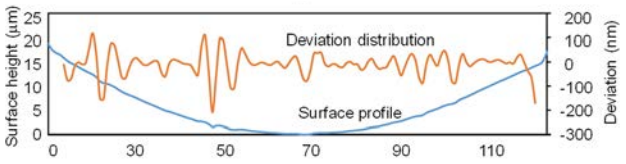

(c)

Fig. 7. SEM micrographs of wet-cut grooves: (a) general view, (b) close-up view, and (c) cross-sectional profile.

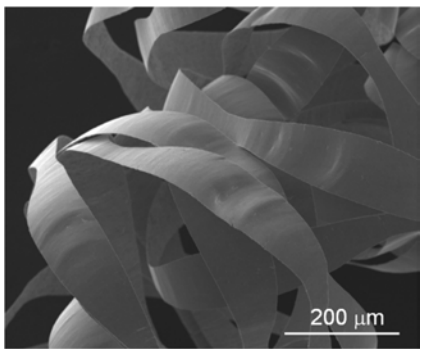

(a)

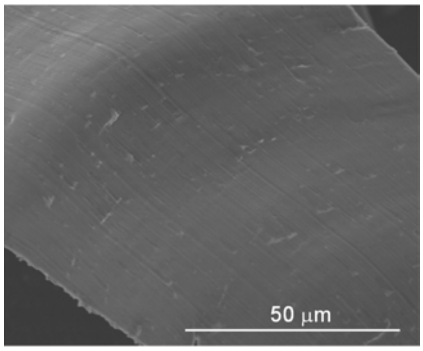

(b)

Fig. 8. SEM micrographs of brass chips in type R groove cutting: (a) general view and (b) close-up view.

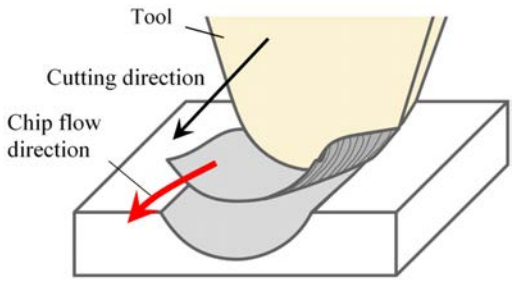

Fig. 9. Schematic of chip flow in brass groove cutting.

shown in **Fig. 9**. However, as shown in **Fig. 8(b)**, their surfaces are not smooth; they have small protrusions. These protrusions might be the result of crystal grains "pulling out" from the groove surface, which corresponds to the formation of deep surface pits.

2.2. Machining Characteristics of OFC

Figure 10(a) is a photograph of a wet-cut roll mold of OFC, and **Fig. 10(b)** is a micrograph of C-type grooves. The grooves have been precisely generated. **Fig. 10(c)** is an SEM micrograph of type C grooves. A smooth surface was obtained (surface roughness < 10 nm *Ra*) without grain boundaries or pit defects. This might be due to the fact that the crystal grains of OFC are purer and finer than those of brass. However, burr formation at the edges of the grooves was confirmed in **Fig. 10(c)**.

Figure 10(d) is a magnified view of the burrs indicated by the white square in **Fig. 10(c)**. The burr formation phenomenon was especially significant when A-type wavy grooves were machined at a large amplitude of *Z*-axis tool oscillation. The lateral faces of the tool contact the side walls of the grooves, causing burr formation [9]. The burr formation phenomenon indicates that OFC has high ductility and low shear strength, which leads easily to the side flow of material.

The chips of OFC collected during the cutting of type R wavy grooves are shown in **Fig. 11**. The magnified views of chip surfaces and lateral surfaces are also shown in the figure. It is clear that the shape and size of the chip units are distinctly different from those of brass chips (**Fig. 8**). The chip units are remarkably shorter, about $1/10$ of the length of a single groove wave and they are significantly thicker. In addition, the lamellar structures seen on the surfaces and sides of the chips are not uniform. These facts indicate that severe plastic deformation and length compression have occurred during chip formation due to the low shear strength of OFC. In addition, interfacial adhesion occurs between the tool rake face and chip, as shown in **Fig. 12**. This chip formation process is unstable and easily causes burr formation on the edges of grooves.

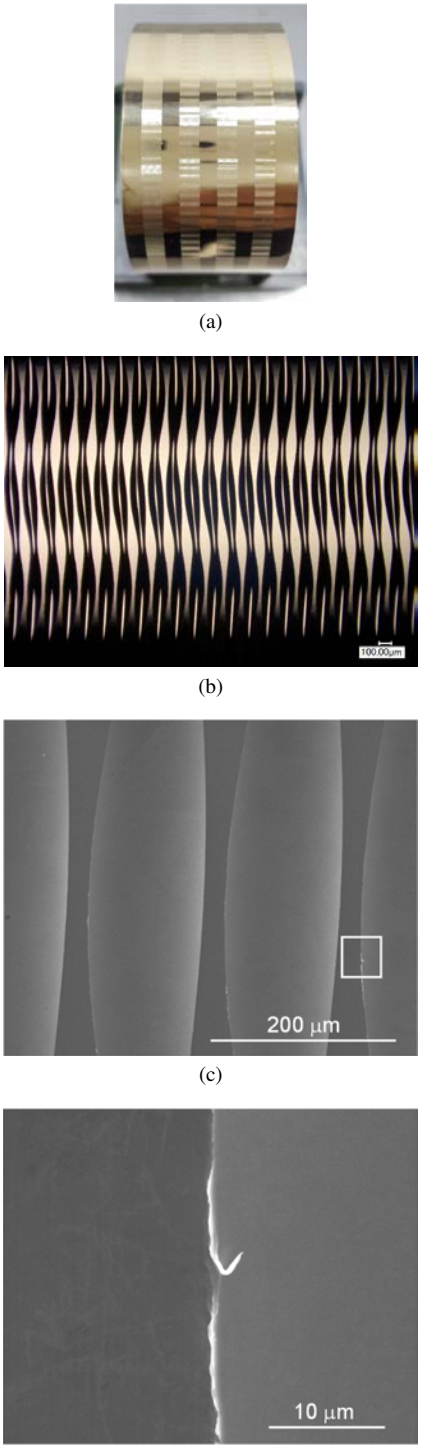

(a)

(b)

(c)

(d)

Fig. 10. (a) A roll mold of OFC, (b) micrograph of type C wavy grooves machined on OFC, (c) SEM micrograph of a groove, and (d) close-up view of burr formation at edge of groove.

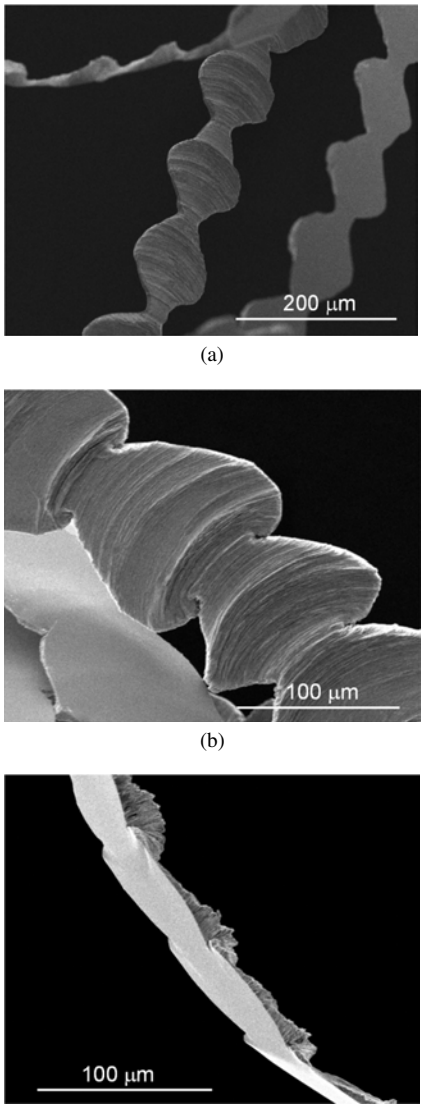

(a)

(b)

(c)

Fig. 11. SEM micrographs of OFC chips in type R groove cutting: (a) general view, (b) close-up view, and (c) side view.

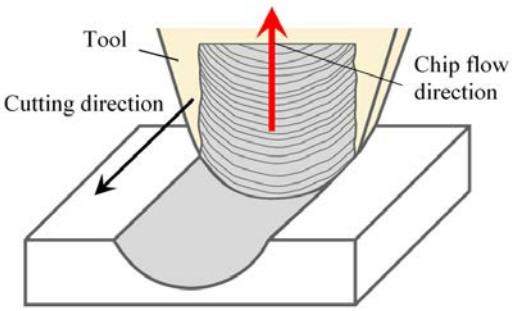

Fig. 12. Schematic of chip flow in OFC groove cutting.

2.3. Machining Characteristics of Aluminum Alloy

Figure 13 is an SEM image of a wavy groove machined dry on aluminum alloy. No grain boundaries or pits are observed on the groove surface; no burr formation is observed at the groove edge. However, many scratch lines are visible on the surface, making it rough. After cutting, the tool was observed with the SEM, and it was found that material adhesions were formed on the cutting edge, as shown in **Fig. 14**. In dry cutting, the affinity of aluminum and the diamond tool surface is high, causing material adhesion. This may act as built-up edges scratching

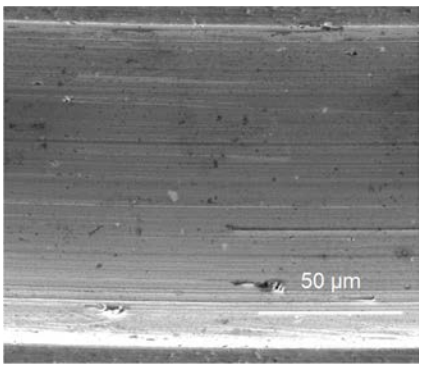

Fig. 13. SEM micrograph of aluminum alloy groove surface in dry cutting.

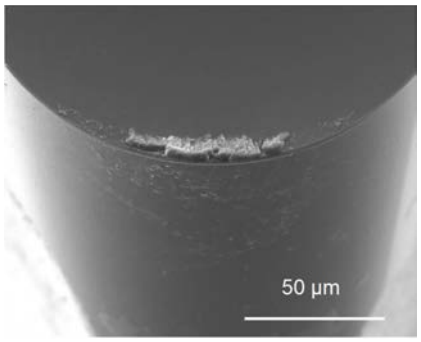

Fig. 14. SEM micrograph of diamond tool edge with material adhesion.

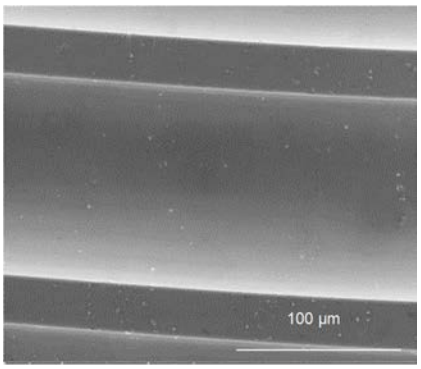

Fig. 15. SEM micrograph of aluminum alloy groove surface in wet cutting.

the surface and leaving parallel lines on it. In wet cutting, however, the material adhesion was suppressed by the lubrication, leaving smooth grooves, as shown in **Fig. 15**. The surface roughness was about 10 nm *Ra*.

Figure 16(a) is an SEM photograph of cutting chips generated during the machining of type A grooves on aluminum alloy. The length of each chip unit is approximately 400 μm, $1/4$ of the length of a single groove wave (1.57 mm). This indicates that the chip flow in this case is smooth, without chip adhesion and accumulation on the tool rake face, as shown in **Fig. 12**. **Figs. 16(b)** and **(c)** are magnified views of chip surfaces and sides. Unlike the

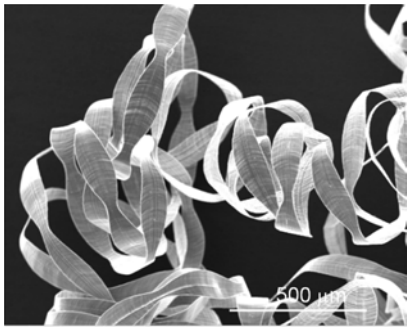

(a)

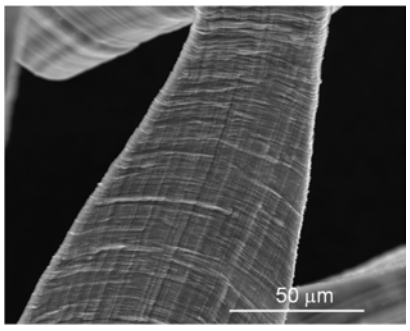

(b)

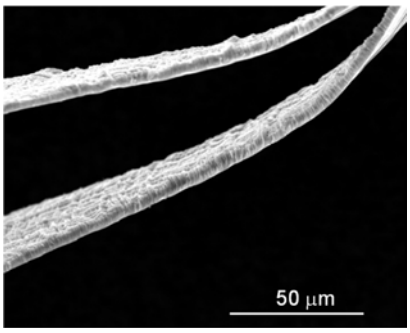

(c)

Fig. 16. SEM micrographs of aluminum alloy chips in type A groove cutting: (a) general view, (b) close-up view, and (c) side view.

chips in **Fig. 8**, the chip surface is very smooth, without protrusions. Also, unlike in **Fig. 11(c)**, the thickness of aluminum alloy chips is very uniform, indicating a stable shear deformation process.

2.4. Wavy-Groove Roll Mold Fabrication

Because of the integrity of the machined surface, aluminum alloy was selected as the most suitable material for roll molds. Finally, a roll mold was fabricated by wet-cutting aluminum alloy. **Fig. 17** is a photograph of the fabricated roll mold. **Fig. 18** shows SEM photographs of various types of microgrooves on the mold surface. The dimensions of the grooves are identical to those in the design in **Table 2**. The cross-sectional profile extracted from the three-dimensional topography measurement results shows that the peak-to-valley form error of the grooves was about 1 μm, and the average surface roughness of the grooves was less than 10 nm *Ra*.

Fig. 17. Photograph of a roll mold of aluminum alloy.

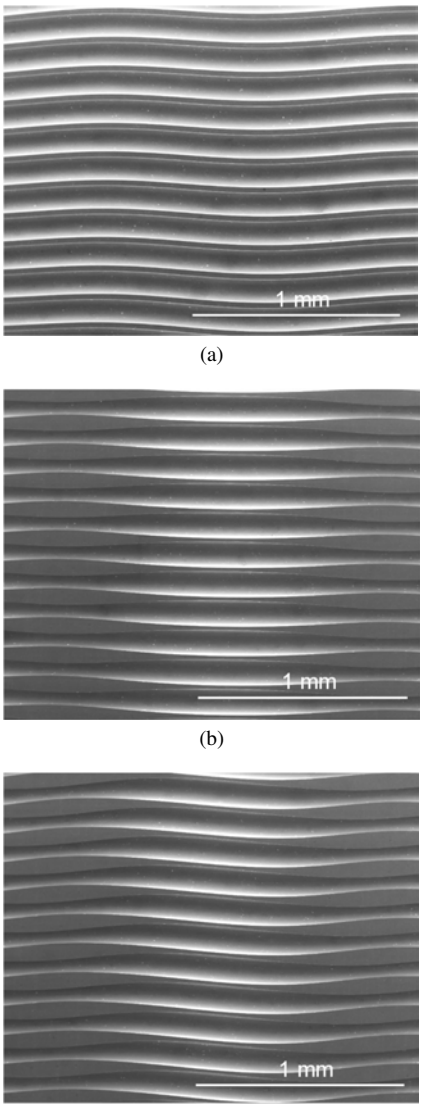

(a)

(b)

(c)

Fig. 18. SEM micrographs wavy grooves machined on aluminum alloy: (a) type A, (b) type R, and (c) type C.

3. Conclusions

Cutting tests of wavy microgrooves were conducted on three metal materials to fabricate roll molds for polymer imprinting. The effects of the workpiece material on chip formation behavior were investigated. The main conclusions can be summarized as follows.

(1) In brass cutting, grain boundary steps and pit defects were significant due to the "pulling out" of crystal grains at a low cutting speed.

(2) In oxygen-free copper cutting, due to the high ductility and low shear strength of the material, burrs formed on the edges of the grooves, and there were large fluctuations in chip thickness.

(3) Aluminum cutting behavior was sensitive to lubrication. In dry cutting, material adhered to the tool rake face, causing surface scratches. In wet cutting, however, a smooth surface was generated, and chips were uniform in thickness.

(4) Two-directional wavy microgrooves were obtained at a 1 μm level form accuracy and a surface roughness of less than 10 nm *Ra*.

References:

[1] D. B. Gregory and B. Bharat, "Fluid drag reduction with shark-skin riblet inspired microstructured surfaces," Advanced Functional Materials, Vol.23, pp. 4507-4528, 2013.
[2] R. Grüneberger, F. Kramer, E. Wassen, W. Hage, R. Meyer, and F. Thiele, "Influence of wave-like riblets on turbulent," Nature-Inspired Fluid Mechanics, Vol.119, pp. 311-329, 2012.
[3] A. A. Hayder, D. M. Hassan, and B. Y. H. Zulkefli, "Bio-inspired passive drag reduction techniques: a review," ChemBioEng Reviews, Vol.2, No.3, pp. 185-203, 2015.
[4] N. Kasagi and Y. Suzuki, "Smart control of turbulence," Trans. of the Institute of Systems, Control and Information Engineers, Vol.48, No.4, pp. 131-137, 2004 (in Japanese).
[5] Y. Luo, Y. Liu, J. Anderson, X. Li, and Y. Li, "Improvement of water-repellent and hydrodynamic drag reduction properties on bio-inspired surface and exploring sharkskin effect mechanism," Applied Physics A, Vol.120, pp. 369-377, 2015.
[6] C. L. Yung, W. C. Hong, and B. H. Fei, "Fabrication of seamless roller mold for continuous roller imprinting of microlens array films," J. of Microelectromechanical Systems, Vol.21, pp. 316-323, 2012.
[7] C. Liu, J. Yan, and S. Lin, "Diamond turning of high-precision roll-to-roll imprinting molds for fabricating subwavelength gratings," Optical Engineering, Vol.55, No.6, 064105, 2016.
[8] L. B. Kong, C. F. Cheung, and W. B. Lee, "A theoretical and experimental investigation of orthogonal slow tool servo machining of wavy microstructured patterns on precision rollers," Precision Engineering, Vol.43, pp. 315-327, 2016.
[9] T. Terabayashi and J. Yan, "Ultra-precision cutting of roll molds having two-directional wavy microstructures," Trans. of the JSME, Vol.85, No.874, 19-00105, 2019 (in Japanese).
[10] M. Mukaida and J. Yan, "Ductile machining of single-crystal silicon for microlens arrays by ultraprecision diamond turning using a slow tool servo," Int. J. of Machine Tools & Manufacture, Vol.115, pp. 2-14, 2017.
[11] D. Wu, P. Zhang, H. Wang, Z. Qiao, and B. Wang, "Effect of cutting parameters on surface quality during diamond turning of micro-prism array," J. of Engineering Manufacture, Proc. of the Institution of Mechanical Engineers Part B, Vol.23, No.3, pp. 555-561, 2017.
[12] J. Yan, T. Oowada, T. Zhou, and T. Kuriyagawa, "Precision machining of microstructures on electroless-plated NiP surface for molding glass components," J. of Materials Processing Technology, Vol.209, pp. 4802-4808, 2009.
[13] K. Asakura and J. Yan, "Water Repellency Control of Oxygen-Free Copper Surface by Diamond-Cut Micro Grooves," Int. J. Automation Technol., Vol.9, No.4, pp. 396-402, 2015.

[14] H. Suzuki, M. Okada, Y. Masuda, Y. Namba, K. Miura, S. Morita, and Y. Yamagata, "Ultraprecision Cutting of Nickel Plated Mold for *X*-Ray Mirror," Int. J. Automation Technol., Vol.10, No.4, pp. 624-631, 2016.
[15] A. Meier, O. Riemer, and E. Brinksmeier, "Diamond Machining of Holograms Using Fine Rectangular Shaped Cutting Tools," Int. J. Automation Technol., Vol.10, No.1, pp. 16-22, 2016.

Name:
Toshitaka Terabayashi

Affiliation:
Graduate Student, Graduate School of Science and Technology, Keio University

Address:
3-14-1 Hiyoshi, Kohoku-ku, Yokohama, Kanagawa 223-8522, Japan

Brief Biographical History:
2017- Graduate School of Science and Technology, Keio University

Main Works:
• Ultraprecision cutting

Name:
Jiwang Yan

Affiliation:
Professor, Department of Mechanical Engineering, Faculty of Science and Technology, Keio University

Address:
3-14-1 Hiyoshi, Kohoku-ku, Yokohama, Kanagawa 223-8522, Japan

Brief Biographical History:
1987-1994 B.E./M.E. Candidate, Jilin University
1994-1996 Ph.D. Candidate, Tsinghua University
1996-2000 Ph.D. Candidate, Tohoku University
2000-2001 Research Associate, Tohoku University
2001-2005 Associate Professor, Kitami Institute of Technology
2005-2012 Associate Professor, Tohoku University
2012- Professor, Keio University

Main Works:
• Ultraprecision machining, micro/nano manufacturing, material processing, and nanomechanics

Membership in Academic Societies:
• Japan Society of Mechanical Engineers (JSME)
• Japan Society for Precision Engineering (JSPE)
• Japan Society for Abrasive Technology (JSAT)
• Japan Society of Applied Physics (JSAP)
• American Society for Precision Engineering (ASPE)
• European Society for Precision Engineering and Nanotechnology (euspen)
• International Academy for Production Engineering (CIRP)